Soft Matter

COMMUNICATION

View Article Online
View Journal | View Issue

Cite this: *Soft Matter*, 2022, **18**, 3644

Received 12th March 2022,
Accepted 27th April 2022

DOI: 10.1039/d2sm00328g

rsc.li/soft-matter-journal

Controlling the dynamics of elastomer networks with multivalent brush architectures†

Michika Onoda, [ab] Fei Jia,[a] Yukikazu Takeoka[b] and Robert J. Macfarlane *[a]

Herein, we report a design strategy for developing mechanically enhanced and dynamic polymer networks by incorporating a polymer with multivalent brush architecture. Different ratios of two types of imidazole functionalized polymers, specifically poly(*n*-butyl acrylate) (PnBA) and poly(poly(*n*-butyl acrylate)) (PPnBA) were blended with Zn(II) ions, thereby forming a series of elastomers with consistent composition but varying network topologies. As the weight fraction of PPnBA increased, the melting temperature, plateau modulus, and relaxation time of the melt increased because of the increase in the crosslinking density and coordination efficiency. Remarkably, however, the activation energy of the flow, E_a, decreased with increasing amounts of PPnBA despite the observed increases in mechanical properties. This unique behavior is attributed to the multivalent nature of the brush polymer, which allows the PPnBA to generate a higher crosslinking density than networks of linear PnBA, even though the brush polymers contain a lower weight fraction of the imidazole crosslinks. This method of lowering E_a, while improving the mechanical properties of the elastomers has great potential in the development of various soft materials such as self-healing or 3D-printable elastomeric structures.

Introduction

Bottlebrush polymers (BBPs) with densely grafted side chains have unique properties that are different from those of conventional linear polymers and loosely grafted polymers because of the combination of their large diameters and unentangled backbones that arise from dense grafting of side chains.[1,2] The physical properties of BBP elastomers can also be easily tuned due to the large number of design variables available, such as side chain density, side chain length, and backbone length.[3] BBPs are thus potentially beneficial for a variety of different functional materials.[4–12] For example, by utilizing their non-entangling characteristics and extremely low overlapping concentration, the crosslinking density of BBP networks can be minimized to produce supersoft elastomers.[6,7] When hard polymer core domains are introduced to both backbone ends of BBPs, elastomers with mechanical properties comparable to those of various biological materials can be synthesized, enabling their application in biological or biomedical studies.[3,9] Furthermore, BBPs have recently been used in the development of self-healing materials,[12] soft sensors,[10] actuators,[8] and 3D-printable materials.[13]

Our group has recently reported the formation of BBP hydrogels by using BBPs as multivalent building blocks; the synthesis of these gels indicated that the BBP architecture potentially leads to unique kinetic behaviors unlike that of similar linear or star polymers.[14,15] For example, poly(ethylene glycol) (PEG)-based BBPs with crosslinkable functional groups at the side chain termini formed gels at a rate 100 times faster than four-arm PEG systems at an equivalent concentration.[14] This increased rate of gel formation was attributed to the BBPs' extremely low overlapping concentration, elongated functionalized side chains, and high multivalency. This result suggests that BBP based self-healing materials with excellent processability can be realized if the exchange reactions between the crosslinks are efficient. However, significant questions remain about how the enhanced formation kinetics in these gels affect the dynamicity of the BBP networks, as well as the relationship between the kinetics of network formation and the mechanical behaviors of these materials. Particularly, the difference in thermodynamic physical properties of polymer networks that contain BBPs as a topologically unique building block compared to linear polymer networks have not been explored.

In this study, we investigate the dynamic physical properties of BBP elastomers crosslinked by noncovalent interactions using rheological techniques to explore the thermodynamics and kinetics of supramolecular-bonded BBPs. Furthermore, by

[a] *Department of Materials Science and Engineering, Massachusetts Institute of Technology, 77 Massachusetts Avenue, Cambridge, Massachusetts 02139, USA. E-mail: rmacfarl@mit.edu*
[b] *Department of Molecular Design and Engineering, Graduate School of Engineering, Nagoya University, Furo-cho, Chikusa-ku, Nagoya, 464-8603, Japan*

† Electronic supplementary information (ESI) available. See DOI: https://doi.org/10.1039/d2sm00328g

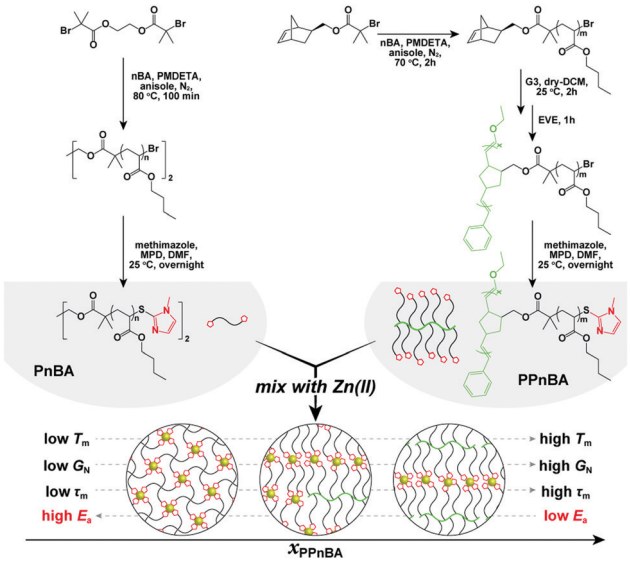

Fig. 1 Conceptual illustration of this study and synthesis of the target polymers. Detailed synthetic procedures are provided in the ESI.†

mixing these BBPs with different amounts of linear polymers that have the same number of repeat units as the BBP side chains, we are able to tune the network topology and examine its effects on elastomer mechanical response (Fig. 1). We demonstrate that introducing a BBP structure can cause the seemingly contradictory effects of simultaneously decreasing the activation energy of flow (E_a) of an elastomer, while also improving its overall mechanical performance. This study provides insight into new synthesis methods to generate rapidly self-healing or readily processable materials using multivalency to alter the dynamics of network formation.

Results and discussion

The target polymers used in this study, poly(*n*-butyl acrylate) (PnBA) and poly(PnBA) (PPnBA), were synthesized using a combination of atom transfer radical polymerization (ATRP) and ring opening metathesis polymerization (ROMP) followed by end-group functionalization through thioesterification (see Fig. 1, Table 1 and Fig. S1–S3, ESI†). The chain length of the linear polymers and the side-arms of the brush polymers were each synthesized to be ~5.5 kDa, as this allowed for the chain length of the network strands to be maintained for different mixtures of polymer types. Detailed synthetic procedures of these polymers are provided in the ESI.† To enable dynamic binding, imidazole-Zn(II) coordination bonds were incorporated into the network as noncovalent bonds. Zn(II) was selected for these investigations as it has the weakest and most dynamic interactions (compared with other investigated metal ions such as Ni(II) and Cu(II)).[16] The target elastomers were prepared by mixing the two imidazole-functionalized polymers, PnBA and PPnBA, in an acetonitrile/dichloromethane (1 : 1 (v/v)) solution containing zinc di[bis(trifluoromethylsulfonyl)imide] (0.25 eq. with respect to imidazole groups), followed by vacuum-drying at 80 °C for 48 h. The mixtures were prepared such that the relative ratio of imidazole and Zn(II) ions was held constant at 4 : 1, regardless of the relative amounts of the brush or linear polymers. This ratio was chosen because it has been previously demonstrated that 4 equivalents of imidazole groups can react with a single Zn(II) ion to produce one crosslinking point.[17] Upon incorporating Zn(II) into the polymer blends, a significant increase in their complex viscosity (Fig. S4, ESI†), absorption peak shift (Fig. S5, ESI†), and Fourier-transform infrared (FT-IR) spectral changes (Fig. S6, ESI†) were observed, indicating successful Zn(II)-imidazole coordination.

The temperature-dependence of the storage modulus (G') and loss modulus (G'') of the PnBA/PPnBA blends was investigated as a function of polymer design (Fig. 2(a)). The melting temperature (T_m) at which G' and G'' cross over was observed to shift to a higher temperature as the PPnBA fraction (x_{PPnBA}, wt%) increased (Fig. 2(b)). For example, the T_m at x_{PPnBA} = 0 was 22.6 °C, while the T_m at x_{PPnBA} = 100 wt% was 39.6 °C. Furthermore, the modulus of the elastomer increased with increasing x_{PPnBA} (Fig. 2(c)). In addition, the temperature-dependence of the moduli above T_m decreased as x_{PPnBA} increased, resulting in highly viscous polymer melts (Fig. S7, ESI†). These changes are hypothesized to result from an

Table 1 Imidazole functionalized polymers synthesized in this study

Sample	Polymer formula[a]	M_n/kDa[b]	$Đ$[c]
PnBA	imi-PnBA$_{45}$-imi	5.8	1.10
PPnBA	P(PnBA$_{41}$-imi)$_{50}$	263	1.09

[a] Abbreviations: imi, 1-methylimidazole; nBA, *n*-butyl acrylate. Numbers following the abbreviations of monomers indicate the average number of repeating units. [b] Number-averaged molecular weight of the polymer. The conversion of the monomer to polymer was calculated based on the decrease in the integrated intensity of the ^{1}H-NMR signal of the double bonds of the unreacted monomer before and after polymerization. [c] Dispersity of polymers, calculated from SEC using tetrahydrofuran as the carrier solvent and calibrated using polystyrene standards.

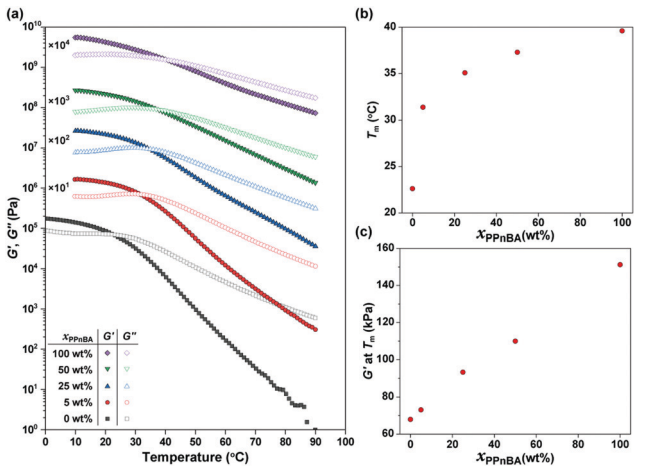

Fig. 2 (a) Temperature-dependence of storage (G') and loss (G'') moduli of PnBA/PPnBA blended elastomers with γ = 1.0% and ω = 10 rad s^{-1}. The data are vertically shifted for clarity using the multiplication factors shown in the plot. (b) Melting temperature (T_m) and (c) G' at T_m of the PnBA/PPnBA elastomer blend as a function of PPnBA fraction (x_{PPnBA}).

increase in the overlapping concentration and crosslinking density with the introduction of densely grafted PPnBA with brush architecture, consistent with prior observations.[18]

The frequency-dependence of the rheological properties of the elastomers were subsequently probed in order to draw a master curve with a reference temperature of 20 °C (Fig. 3(a)), thereby enabling better examination of how additional BBP quantities affected material mechanical response. In the lower frequency regime, G' was smaller than G'', and the slopes of the G' and G'' curves for the x_{PnBA} = 100 wt% material in this regime were 2 and 1, respectively, representing the typical rheological behavior of a viscoelastic fluid. However, the slope of the curves decreased as x_{PPnBA} increased, indicating a transformation to highly viscous polymer melts; the slopes of the G' and G'' curves at x_{PPnBA} = 100 wt% were 0.89 and 0.73, respectively (Fig. S8, ESI†). These different slopes of G' and G'' are common to non-Newtonian fluids of high-molecular-weight polymer melts.[19] This behaviour can be explained by the fact that PPnBA has fifty times higher molecular weight and lower overlapping concentration[14] compared to PnBA. Furthermore, the PPnBA, which possesses a greater surface area and larger number of imidazole groups per polymer, would be expected to diffuse more slowly as a result of this larger number of potential points of attachment between adjacent bottlebrush polymers.[20]

For elastomeric samples, the relaxation time of melts (τ_m) can be calculated from their angular frequency at the cross-over point (ω_m):

$$\tau_m = \frac{2\pi}{\omega_m}. \quad (1)$$

In the samples investigated here, τ_m was found to increase from 0.85 to 5.16 s as x_{PPnBA} increased from 0 to 100 wt% (Fig. 3(b)), indicating that the building blocks of the elastomer became less dynamic as x_{PPnBA} increased. This result can be attributed to the effect of the multivalency and conformation of PPnBA. As the average number of the functional groups per polymer increases, more energy is required for each building block to be mobile. Moreover, as the population of stretched poly(*n*-butyl acrylate) chains increases, coordination efficiency of the building blocks increases as well.

Using these data, the plateau moduli (G_N) of the networks were estimated to gain insights into the effect of blending of linear and brush polymers on crosslinking density and coordination efficiency (p). Due to the non-uniform distribution of building blocks in blended systems, we applied a 'minimum' method[21] to estimate G_N, as follows:

$$G_N = G'(\omega)_{G' \to \text{minimum}} \quad (2)$$

where the plateau modulus is taken to coincide with the storage modulus at the minimum of G'' in the rubbery plateau region of the material. Thus, G_N was found to increase monotonically with increasing x_{PPnBA} (Fig. 3(c)), and the G_N at x_{PPnBA} = 100 wt% was four times higher than the G_N at x_{PPnBA} = 0 wt%. This behavior is also clearly observed in the van Gurp–Palmen plots (vGP-plot)[22] which denote the absolute values of the complex shear modulus (G^*) against phase angles (δ) (Fig. 3(d)). G^* at the minimum value of δ is correlated to the plateau modulus. Instead of eqn (2), the alternative expression of G_N is given as:[23]

$$G_N = G^*(\delta)_{\tan\delta \to \text{minimum}} \quad (3)$$

Thus, an increase in the complex modulus at the minimum phase angle with increasing x_{PPnBA} represents an increase in G_N.

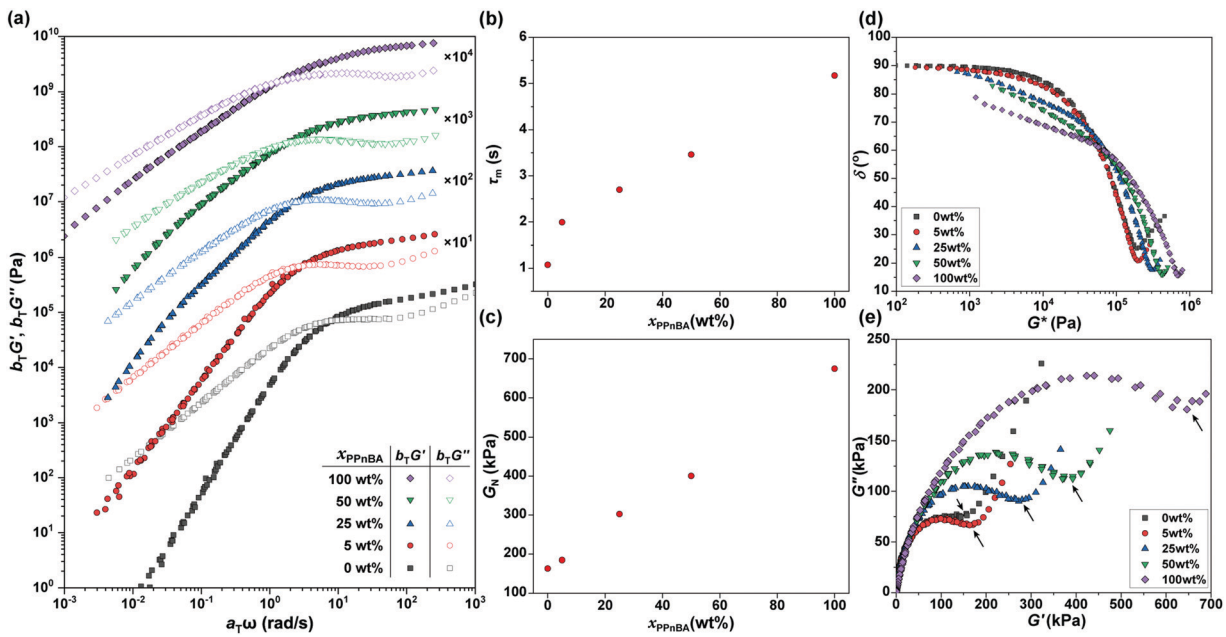

Fig. 3 (a) Master curves of storage (G') and loss (G'') moduli for PnBA/PPnBA blended elastomers at the reference temperature of 20 °C. The data are vertically shifted for clarity using the multiplication factors shown in the plot. (b) Relaxation time of the melt (τ_m) and (c) plateau modulus (G_N) for the PnBA/PPnBA elastomer blend as a function of PPnBA fraction, x_{PPnBA}. (d) van Gurp–Palmen plots and (e) Cole–Cole plots of the PnBA/PPnBA elastomer blends.

This increase in G_N can be attributed to the increase in the average branch number, which results in an increase in the number density of elastically effective network strands (ν) and coordination efficiency (p) supported by the extended side chains. Indeed, by estimating the ν and p *via* the simple affine network model, we found that both ν and p increased as x_{PPnBA} increased (Fig. S9 and S10, ESI†). Based on these results, we conclude that T_m, τ_m, and G_N increase with increasing x_{PPnBA}, owing to the formation of a robust network.

In addition, considering that the elastomers are composed of two polymer components with large differences in their molecular weights and local imidazole group densities, the distribution of the relaxation time is influenced by x_{PPnBA}. To assess the effect of x_{PPnBA} on the relaxation time, we employed Cole–Cole plots, which are a plots of G' against G''.[24] In general, a polymer blend shows two arcs in the Cole–Cole plots owing to the existence of two relaxation modes.[25] As shown in Fig. 3(e), all the PnBA/PPnBA elastomer samples exhibit two arcs, even at x_{PPnBA} = 0 wt% (*i.e.*, for pure PnBA elastomer). This result suggests that the PnBA elastomer involves the relaxation of the imidazole-Zn(II) dynamic bonds in addition to the relaxation of polymer motion. Furthermore, as x_{PPnBA} increased, the local minimum in the Cole–Cole plot (see the arrows) shifted to the high-viscosity region. This shift suggests that the elastomer has an additional relaxation mode related to the motion of PPnBA.[25] Because the percolation of the PPnBA network proceeds with increasing x_{PPnBA}, the upturn was found to significantly shift to the high-viscosity region at x_{PPnBA} = 100 wt%. The existence of multiple relaxation processes was also indicated in the vGP-plot (Fig. 3(d)) as a gradual increase in δ as G^* decreases with increasing x_{PPnBA}.[26,27] The fact that PnBA and PPnBA elastomers have different relaxation modes motivated us to gain further insights into the thermodynamics of these dynamic polymer interactions, which are predicted to be key to the use of BBPs for self-healing and processable materials.

We therefore estimated the activation energy of flow associated with the glass transition process, E_a, *via* Arrhenius analysis[28] of the viscoelastic response:

$$a_T = A \exp\left(\frac{E_a}{R}\left(\frac{1}{T} - \frac{1}{T_{ref}}\right)\right). \quad (4)$$

Remarkably, despite the increase in mechanical properties noted above with increasing x_{PPnBA}, E_a was actually found to decrease with increasing x_{PPnBA} (Fig. 4). E_a was 86 kJ mol^{-1} at x_{PPnBA} = 0 wt%, decreasing to 75 kJ mol^{-1} at x_{PPnBA} = 100 wt%. These results may seemingly be contradictory. However, they can be rationalized by comparing the different topologies of the linear and brush polymers.

While G_N is positively related to the number density of elastically effective network strands, E_a is positively related to the number density of imidazole-Zn(II) coordination bonds that should be broken to acquire fluidity. Here, both chain ends of the linear PnBA are functionalized with imidazole groups. On the other hand, only one end of each side chain of PPnBA is functionalized with an imidazole group, while the other end is covalently bound to the backbone. Therefore, although the number of network strands of both the PnBA and PPnBA networks are equivalent in molecular weight, the concentration of the imidazole groups ([imi]) in each network is different. Indeed, as x_{PPnBA} increased, [imi] decreased monotonically (Fig. 4). Further, the increase of x_{PPnBA} led to the increase of coordination bonds between adjacent side chains, considering the densely grafted polymer architecture of PPnBA. We would note that intramolecular coordination of linear PnBA is negligible because the molecular weight of PnBA is five times smaller than the entanglement molecular weight of PnBA.[29] Therefore, while imidazole-Zn coordination between adjacent side chains of PPnBA can decrease E_a, this coordination events can still contribute as mechanically effective crosslinking points because each Zn(II) ion can potentially interact with four imidazole groups.

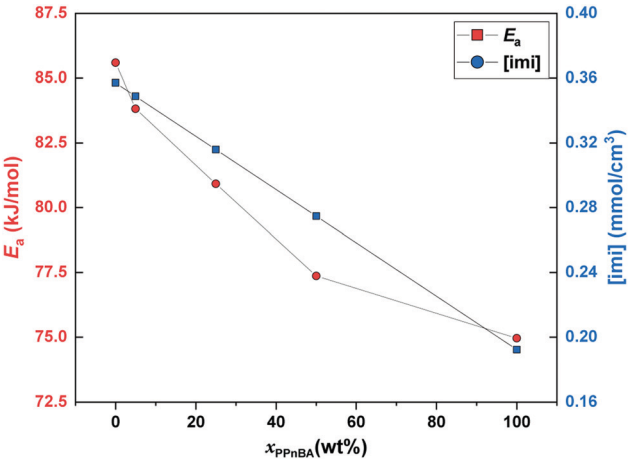

Fig. 4 Activation energy of flow (E_a) and mole density of imidazole groups ([imi]) as a function of PPnBA fraction, x_{PPnBA}.

While the introduction of the brush structure leads to an increase in crosslinking density and thus increased G_N, it also leads to a decrease in the number of imidazole-Zn(II) bonds per mass of polymer that need to be broken to enable the material to flow, resulting in the decrease of E_a. Additionally, it should be noted that while [imi] has a linear relationship with x_{PPnBA}, E_a showed an initially rapid decrease followed by a slower decrease as the PPnBA wt% increased. The rapid decrease of E_a can be considered the effect of intramolecular coordination. On the other hand, the increase of x_{PPnBA} leads to increased crosslinking density and coordination efficiency of the building blocks, increasing mechanical stiffness. A slower decrease of E_a would therefore be observed because the network stiffening inhibits the pulling-out of the network strands from imidazole-Zn(II) coordination points.

In general, the activation energy of flow can be referred to as an indicator of processability and self-healing property of the materials. Thus, we conclude that the design strategy of multivalent binding between brush polymers can enhance the bulk material modulus while decreasing E_a could in principle be used to simultaneously improve the processability and mechanical properties of polymeric materials.

Conclusions

In this study, we investigated the physical properties of PnBA/PPnBA mixed elastomers using rheological techniques. As x_{PPnBA} increased, T_m, G_N, and τ_m increased as a result of the multifunctionality of the PPnBA unit, which increased the crosslinking density, but surprisingly decrease E_a. This seemingly contradictory behavior can be attributed to the use of brush polymers causing a decrease in the number density of imidazole groups, but also an increasing in the density of crosslinks. Decreasing E_a is essential for increasing processability of self-healing materials and to ultimately achieve self-healing under ambient conditions. Current self-healing elastomers that include dynamic molecular interactions often sacrifice mechanical robustness in order to achieve processability. Our methodology represents a potential method to achieve processability without compromising mechanical strength and is amenable for methods to further control mechanical properties by controlling the type of binding group, degree of polymerization, or polymer functionality. This design principle should prove useful in developing elastomers with self-healing properties, as such materials often require dynamic molecular interactions that make it difficult to balance mechanical robustness and processability.[17,30]

Author contributions

M. O. performed all experiments and authored the manuscript. F. J., Y. T., and R. J. M. conceived the study, as well as authored the manuscript.

Conflicts of interest

There are no conflicts to declare.

Acknowledgements

This work was supported by a NSF CAREER grant, Award Number CHE-1653289. This work is supported by the MRSEC Program of the National Science Foundation under award DMR 1419807 and made use of the MRSEC Shared Experimental Facilities at MIT, and the JSPS KAKENHI Grant Numbers 16J09350 and 20K15341.

References

1 R. Verduzco, X. Li, S. L. Pesek and G. E. Stein, *Chem. Soc. Rev.*, 2015, **44**, 2405–2420.
2 S. L. Pesek, X. Li, B. Hammouda, K. Hong and R. Verduzco, *Macromolecules*, 2013, **46**, 6998–7005.
3 M. Vatankhah-Varnosfaderani, W. F. M. Daniel, M. H. Everhart, A. A. Pandya, H. Liang, K. Matyjaszewski, A. V. Dobrynin and S. S. Sheiko, *Nature*, 2017, **549**, 497–501.
4 D. Neugebauer, Y. Zhang, T. Pakula, S. S. Sheiko and K. Matyjaszewski, *Macromolecules*, 2003, **36**, 6746–6755.
5 T. Pakula, Y. Zhang, K. Matyjaszewski, H. Lee, H. Boerner, S. Qin and G. C. Berry, *Polymer*, 2006, **47**, 7198–7206.
6 L. Cai, T. E. Kodger, R. E. Guerra, A. F. Pegoraro, M. Rubinstein and D. A. Weitz, *Adv. Mater.*, 2015, **27**, 5132–5140.
7 W. F. M. Daniel, J. Burdyńska, M. Vatankhah-Varnoosfaderani, K. Matyjaszewski, J. Paturej, M. Rubinstein, A. V. Dobrynin and S. S. Sheiko, *Nat. Mater.*, 2016, **15**, 183.
8 M. Vatankhah-Varnoosfaderani, W. F. M. Daniel, A. P. Zhushma, Q. Li, B. J. Morgan, K. Matyjaszewski, D. P. Armstrong, R. J. Spontak, A. V. Dobrynin and S. S. Sheiko, *Adv. Mater.*, 2017, **29**, 1604209.
9 M. Vatankhah-Varnosfaderani, A. N. Keith, Y. Cong, H. Liang, M. Rosenthal, M. Sztucki, C. Clair, S. Magonov, D. A. Ivanov, A. V. Dobrynin and S. S. Sheiko, *Science*, 2018, **359**, 1509–1513.
10 V. G. Reynolds, S. Mukherjee, R. Xie, A. E. Levi, A. Atassi, T. Uchiyama, H. Wang, M. L. Chabinyc and C. M. Bates, *Mater. Horizons*, 2019, **7**, 181–187.
11 M. Abbasi, L. Faust and M. Wilhelm, *Adv. Mater.*, 2019, **31**, 1806484.
12 J. L. Self, C. S. Sample, A. E. Levi, K. Li, R. Xie, J. R. de Alaniz and C. M. Bates, *J. Am. Chem. Soc.*, 2020, **142**, 7567–7573.
13 R. Xie, S. Mukherjee, A. E. Levi, V. G. Reynolds, H. Wang, M. L. Chabinyc and C. M. Bates, *Sci. Adv.*, 2020, **6**, eabc6900.
14 F. Jia, J. M. Kubiak, M. Onoda, Y. Wang and R. J. Macfarlane, *Adv. Sci.*, 2021, **8**, e2100968.
15 F. Jia, J. Song, J. M. Kubiak, M. Onoda, P. J. Santos, K. Sano, N. Holten-Andersen, K. Zhang and R. J. Macfarlane, *Chem. Mater.*, 2021, **33**, 5748–5756.
16 J. E. Bauman and J. C. Wang, *Inorg. Chem.*, 1964, **3**, 368–373.
17 D. Mozhdehi, S. Ayala, O. R. Cromwell and Z. Guan, *J. Am. Chem. Soc.*, 2014, **136**, 16128–16131.
18 J. Paturej and T. Kreer, *Soft Matter*, 2017, **13**, 8534–8541.
19 O. O. Mykhaylyk, C. M. Fernyhough, M. Okura, J. P. A. Fairclough, A. J. Ryan and R. Graham, *Eur. Polym. J.*, 2011, **47**, 447–464.
20 A. Shabbir, H. Goldansaz, O. Hassager, E. van Ruymbeke and N. J. Alvarez, *Macromolecules*, 2015, **48**, 5988–5996.
21 C. Liu, J. He, E. van Ruymbeke, R. Keunings and C. Bailly, *Polymer*, 2006, **47**, 4461–4479.
22 M. van Gurp and J. Palmen, *Rheol. Bull.*, 1998, **67**, 5–8.
23 Z. Qian and G. B. McKenna, *Polymer*, 2018, **155**, 208–217.
24 T. Mezger, *The Rheology Handbook*, Vincentz Network, Hanover, Germany, 2020.
25 D. Wu, L. Wu, Y. Sun and M. Zhang, *J. Polym. Sci., Part B: Polym. Phys.*, 2007, **45**, 3137–3147.
26 S. Trinkle and C. Friedrich, *Rheol. Acta*, 2001, **40**, 322–328.
27 M. A. Kanso and A. J. Giacomin, *Phys. Fluids*, 2020, **32**, 033101.
28 F. Tanaka and S. F. Edwards, *J. Non-Newton Fluid*, 1992, **43**, 247–271.
29 J. D. Tong and R. Jerôme, *Polymer*, 2000, **41**, 2499–2510.
30 Y. Chen, A. M. Kushner, G. A. Williams and Z. Guan, *Nat. Chem.*, 2012, **4**, 467–472.

